ACS APPLIED POLYMER MATERIALS

pubs.acs.org/acsapm

Article

Inverse Vulcanization with SiO_2-Embedded Elemental Sulfur for Superhydrophobic, Anticorrosion, and Antibacterial Coatings

Congcong Miao, Xingwei Xun, Liam J. Dodd, Shiquan Niu, Haoran Wang, Peiyao Yan, Xi-Cun Wang, Jian Li,* Xiaofeng Wu,* Tom Hasell,* and Zheng-Jun Quan*

Cite This: https://doi.org/10.1021/acsapm.2c00490

Read Online

ACCESS | Metrics & More | Article Recommendations | Supporting Information

ABSTRACT: Sulfur-rich polymers generated from the inverse vulcanization of elemental sulfur with unsaturated monomers have emerged as a family of organic polymers with unique functionalities and broad potential applications. First described in 2013, inverse vulcanization is still in its infancy regarding its fundamental development, property exploration of the resultant polymers, and practical utilizations. Herein, the robust properties of sulfur-rich composites generated by inverse vulcanization with SiO_2-embedded elemental sulfur are revealed, furnishing superhydrophobicity with static water contact angles of up to 154.7 ± 1.8°, a high anticorrosive effect of 98.9% protection efficiency for Mg alloy in 3.5 wt % NaCl solution, and a good antibacterial performance against *Escherichia coli* (81%) and *Staphylococcus aureus* (75%). The resulted composite also shows excellent self-cleaning functionalities. This has not only expanded the properties/functionalities and applications of the sulfur-rich polymers resulting from inverse vulcanization but also provided low-cost alternatives to superhydrophobic coating materials for practical applications.

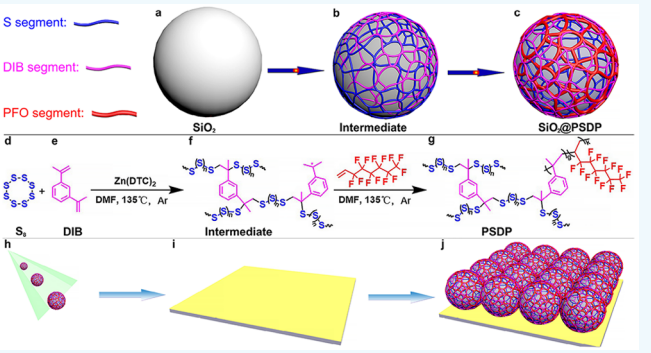

KEYWORDS: *sulfur-rich polymers, self-cleaning, inverse vulcanization, superhydrophobic*

1. INTRODUCTION

As a family of organic polymers, sulfur-rich polymers generated from inverse vulcanization with elemental sulfur (S_8), by-products of the petrol and nature gas industries with over 70 million tons of production annually, are of significantly growing interest for their unique functionalities and potential applications.[1,2] Since the pioneering work demonstrated by Pyun and co-workers in 2013,[3] many efforts have contributed to the development of inverse vulcanization, recognizing the properties of the resultant polymers as well as exploring their practical applications.[4−10] Therefore, the applications of these sulfur-rich polymers have been investigated extensively. They are promising and have advantages in many aspects due to the interesting structural components and functionalities distinguished from the carbon-based polymers, such as environmental protection and rectification,[11] noble metals recovery,[12−17] Li−S batteries,[18−26] fertilizers,[27,28] optical devices,[29,30] and healable/self-healable polymeric materials,[31−33] in addition to many applications still to be explored.

Of particular note is that the sulfur-rich polymers inherit the activity of elemental sulfur against some bacteria and microorganisms, facilitating their applications in antibacterial and anticorrosive materials much more feasibly than their carbon-based counterparts. Only a few examples show the antibacterial property of sulfur-rich polymers and their applications up to date. Thus, Lienkamp et al. demonstrated that a smooth film obtained by spin coating a poly(S-DIB) copolymer dissolved in 1,4-dichlorobenzene solution possessed biological activity. Obvious microphase separation (<60 wt % S) was observed when the polymer's carbon-containing repeating units separated to the air−polymer interface, resulting in the polymer coating being hydrophobic and capable of killing *Escherichia coli* (*E. coli*).[34] Hasell et al. investigated those blended copolymers of poly(S-DIB) and poly(S-DCPD) have bactericidal effects to *E. coli*, while the sole poly(S-DIB) has a bactericidal effect to *Staphylococcus aureus* (*S. aureus*) instead.[35]

On the other hand, microorganisms dominated the degradation and/or failure of organic coatings of ship hulls and sea equipment in the ocean, limiting the effectivity of anticorrosion coatings in hostile marine environments. Circumventing the formation of biofilms on the coating of ship hulls and pipelines is also of extensive importance in the

Received: March 21, 2022
Accepted: May 19, 2022

Scheme 1. Preparation Diagram of SiO_2@PSDP: (a) SiO_2, (b) Intermediate, (c) SiO_2@PSDP, (d) the Chemical Reaction Equations of (f) Intermediate and (g) SiO_2@PSDP, (h) Representative Airbrush, (i) Adhesive Spraying, and (j) Artificial Structured Coating

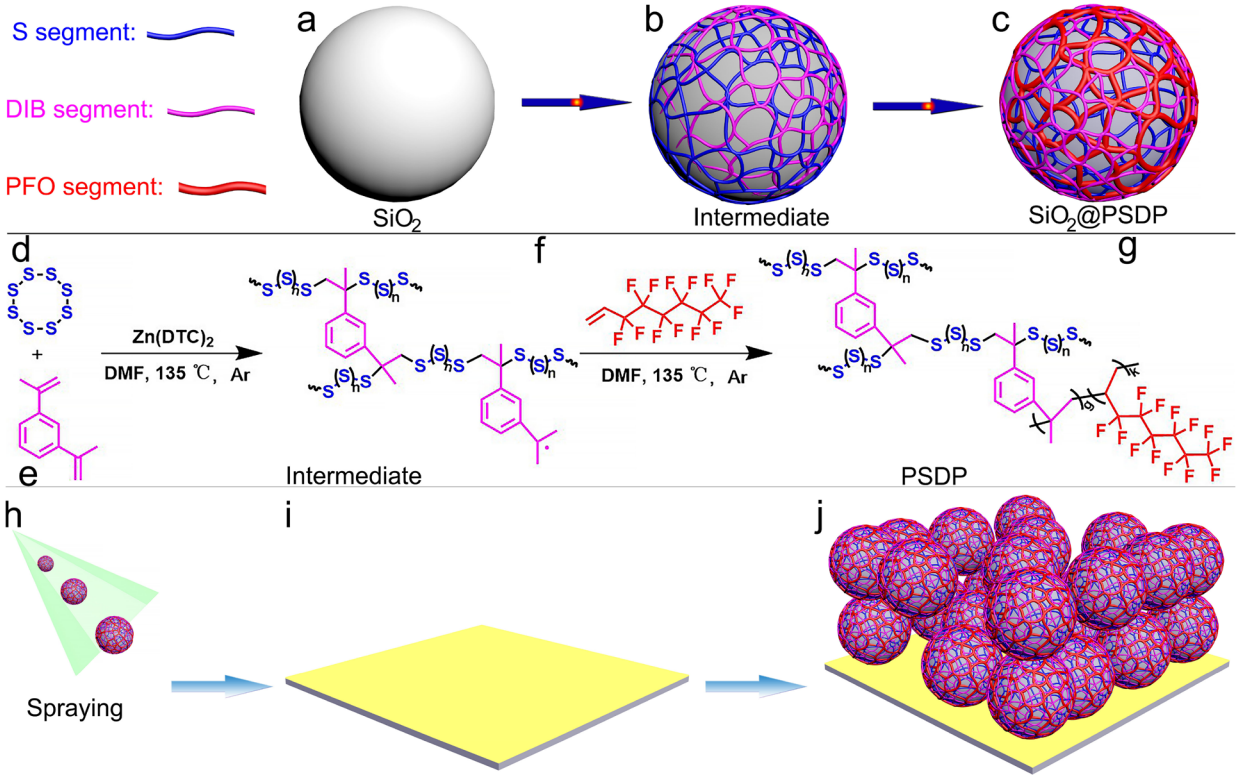

marine industry.[36−38] Meanwhile, the superhydrophobic surfaces are immersed in a polar solvent or a corrosive medium, and they may spontaneously form an air layer between the liquid−solid interface according to the anticorrosion mechanism.[39] When the superhydrophobic surface adheres to some bacteria or microorganisms, these surfaces induce the water droplets to roll or rotate as the polar water droplets cannot be attached, eliminating the bacteria just landed or causing them to burst. Although these antiadhesive surfaces are able to oppose or restrain cell adhesion, they are insufficient for reducing the growth of microorganisms.[40−42] Therefore, the development of a functional anticorrosive coating with both superhydrophobic and antibacterial properties is still inevitably demanded.

Herein, a strategy to develop superhydrophobic, antibacterial, and anticorrosive composite materials derived from the sulfur-rich polymers generated by the inverse vulcanization with SiO_2-embedded elemental sulfur tailored with a hydrophobic functional group was investigated for the first time, and the resultant composites show superhydrophobicity, with good to excellent antibacterial and anticorrosive properties. The tests were carried out with nanoparticles of obtained sulfur-rich composites sprayed onto glass slide and/or magnesium alloy surfaces. SiO_2 nanoparticles (SiO_2) were used to construct micro-/nanoroughness. S_8, 1,3-diisopropenylbenzene (DIB) and 1*H*,1*H*,2*H*-perfluoro-1-octene (PFO) were coated onto SiO_2 in the order of sequence to form the coating SiO_2@Poly(S-DIB-PFO) (SiO_2@PSDP). The adhesive spraying (3M 75) was used to improve the binding force of SiO_2@PSDP with the glass slide and magnesium alloy surface.

The schematic illustration of the preparation process and the microscopic morphology of SiO_2@PSDP are shown in Scheme 1. Parts a and b of Scheme 1 represent the SiO_2 and intermediate, in which the blue and magenta network structure demonstrates S_8 and the DIB segment in SiO_2@PSDP, respectively. Scheme 1c illustrates SiO_2@PSDP, where the red network structure represents the PFO segment in SiO_2@PSDP.

2. EXPERIMENTAL DETAILS

2.1. Materials and Characterizations. Sulfur (S_8 or S, sublimed powder, ≥ 99.5%, Shanghai Chemical Reagent Co. Ltd., China), 1,3-diisopropenylbenzene (DIB, > 97.0%, Shanghai Aladdin Biochemical Technology Co. Ltd., China), 1*H*,1*H*,2*H*-perfluoro-1-octene (PFO, 98.0%, Shanghai Titan Scientific Co. Ltd., China), zinc diethyldithiocarbamate ($Zn(DTC)_2$, >99%, Shanghai Titan Scientific Co., Ltd., China), myrcene (90%, Rowen Reagent Co. Ltd., China), dicyclopentadiene (DCPD, 98.0%, Tansoole Co. Ltd., China), 1-octene (98%, Aladdin Chemistry Co. Ltd., China), 2,2,6,6-tetramethylpiperidinooxy (TEMPO, 98%, Shanghai Titan Scientific Co. Ltd., China), 2,6-di-*tert*-butyl-4-methylphenol (BHT, 99%, Shanghai Titan Scientific Co. Ltd., China), chloroform-*d* ($CDCl_3$, 99.8 atom % D, stab. with Ag, cont. 0.03 V/V % TMS, Ningbo Cuiying Chemical Technology Co. Ltd., China), dimethyl sulfoxide-d_6 (DMSO-d_6, 99.8 atom % D, TMS, Energy Chemical Co. Ltd., China), SiO_2 nanoparticles (SiO_2, 15−20 nm, >99.5%, Shanghai Aladdin Biochemical Technology Co. Ltd., China), beer extract (Beijing Shuangxuan Microbial Culture Medium Product Factory), agar powder (Beijing Solarbio Science & Technology Co. Ltd., China), peptone proteose (Shanghai Zhongqin Chemical Reagent Co. Ltd., China), sodium chloride (Yantai Shuangshuang Chemical Co. Ltd., China), adhesive spray (AS, 3M75, 3M Co. Ltd., China), and absolute ethyl alcohol (99.7%, Sinopharm Group Chemical Reagent Co. Ltd., China) were used.

Nuclear magnetic resonance (NMR, Varian Mercury Plus 400 and Agilent DD2−600 MHz, USA), X-ray photoelectron spectroscopy

https://doi.org/10.1021/acsapm.2c00490
ACS Appl. Polym. Mater. XXXX, XXX, XXX−XXX

(XPS, Thermo ESCALAB 250XI). Fourier-transform infrared (FTIR, Digilab FTS-3000, USA), and X-ray energy dispersive spectrometer (EDS, Oxford INCA, X-MAX50, England) were used. Powder X-ray diffraction (PXRD, Rigaku D/Max-2200PC, Japan) patterns of S_8, polymers, and composites were characterized using Cu Kα radiation (λ = 1.5418 Å) at 40 kV, 100 mA, and scanning range from 5° to 80°. Differential scanning calorimetry (DSC, TAQ2000, USA, and Discovery series DSC25, TA Instruments) was conducted at constant heating and cooling rates of 10 °C min^{-1} under N_2 atmosphere in the range from −50 to +150 °C. Thermogravimetric analysis (TGA, Mettler Toledo TGA/DSC1, Switzerland) was performed in N_2 and flowed from 25 to 800 °C at a rate of 10 °C min^{-1}. The water contact angle (WCA) was measured with a SL200 KB apparatus at ambient temperature. The electrochemical workstation (ChenhuaCHI660E, Shanghai) tested the anticorrosion performance of coatings, and the scanning rate of the Tafel potentiodynamic polarization curve was 10 mV/s.

2.2. Synthesis of SiO_2@Poly(S-DIB). To a 100 mL Schlenk tube equipped with a magnetic stir bar was added SiO_2 (50 mg) in DMF (9 mL), and the mixture was treated with ultrasound for 15 min at 25 °C. After the addition of S_8 (256 mg, 1 mmol) and $Zn(DTC)_2$ (7 mg, 1.5 wt %), the reaction tube was sealed and degassed thoroughly with argon, connecting with the tail gas absorption tube to the branch of the Schlenk tube. When a yellow homogeneous dispersed solution was appeared from the mixture with heating at 135 °C, DIB (159 mg) in DMF (1 mL) was injected into the mixture by syringe, followed by a quick degassing with argon again. The mixture was then reacted for 5 h at the same temperature. The obtained mixture was settled out with ethanol after cooling down, named as SiO_2@Poly(S-DIB) and abbreviated as SiO_2@PSD. In addition, various ratios of SiO_2, S_8, $Zn(DTC)_2$, and DIB were applied for comparison while other conditions were maintained.

2.3. Synthesis of SiO_2@Poly(S-DIB-PFO). To a 100 mL Schlenk tube equipped with a magnetic stir bar were added SiO_2 (120 mg) and DMF (8 mL), and the mixture was treated with ultrasound for 15 min at 25 °C. After the addition of S_8 (358 mg, 1.4 mmol) and $Zn(DTC)_2$ (8 mg, 1.5 wt %), the reaction tube was sealed and degassed thoroughly with argon, connecting with the tail gas absorption tube to a branch of the Schlenk tube. When a yellow homogeneous dispersed solution appeared from the mixture with heating at 135 °C, DIB (159 mg) in DMF (1 mL) was injected into the mixture by syringe, followed by a quick degassing with argon again. The mixture was reacted for 5 h at the same temperature. Then PFO (346 mg, 1 mmol) in DMF (1 mL) was injected into the mixture by syringe followed by quickly degassing with argon again, and the resultant mixture was reacted for another 5 h at the same temperature. The obtained mixture was settled out with ethanol after cooling down, named as SiO_2@Poly(S-DIB-PFO) and abbreviated as SiO_2@PSDP. In addition, various ratios of SiO_2, S_8, $Zn(DTC)_2$, DIB, and PFO were applied for comparison while other conditions were maintained.

2.4. Synthesis of Poly(S-DIB-PFO). A 100 mL Schlenk tube equipped with a magnetic stir bar was sealed after the addition of S_8 (358 mg, 1.4 mmol) and $Zn(DTC)_2$ (8 mg, 1.5 wt %), in which the air was cleared away using argon, connecting with the tail gas absorption tube to the branch of the Schlenk tube. When a yellow homogeneous solution appeared at 135 °C from the mixture, DIB (159 mg, 1 mmol) in DMF (9 mL) was injected into the mixture by syringe, followed by a quick degassing with argon again. The mixture was reacted for 5 h at the same temperature. Then PFO (346 mg) in DMF (1 mL) were injected by syringe into the mixture with degassing, and the resultant mixture was reacted for another 5 h at the same temperature. After cooling down, the mixture was precipitated in ethanol, filtered, washed with ethanol, and dried at 60 °C for direct use later, named as Poly(S-DIB-PFO), abbreviated as PSDP.

2.5. Sprayed onto a Coating. Poly(S-DIB), SiO_2@PSD, SiO_2@PSDP, SiO_2, SiO_2@S, SiO_2@Poly(DIB), SiO_2@Poly(PFO), SiO_2@Poly(DIB-PFO), SiO_2@Poly(S-Myrcene-PFO), SiO_2@Poly(S-DCPD-PFO), and SiO_2@Poly(S-DIB-Octene) are dispersed in the ethanol solution. After the addition of the resultant dispersion (5 mL) to the HD-130 (0.3 mm) type airbrush which is connected to the U-601G type air pump, the targeted glass slide previously sprayed with 3M 75 glue was then evenly sprayed with these dispersed nanoparticles in solution by the air pump, and the slide was dried at 60 °C for 6 h to measure the WCA of resultant coatings afterward.

2.6. Self-Cleaning Experiment. In order to test the self-cleaning performance of the prepared SiO_2@PSDP coating, the prepared nanoparticles were sprayed on a glass slide, which was dried at 60 °C for 6 h without any further treatments; the resultant glass slide was tilted on a watch glass and sprinkled with a certain amount of sand. The water droplets were then dropped onto the coating surface to remove the sand, verifying the self-cleaning property of the coating. The self-cleaning performance of the coatings by water droplets was recorded by a digital camera (see the Supporting Information for details).

2.7. Peeling Test. The commercially available 3M 810 test tape was pasted onto the coating, and a certain pressure was applied on the back of the test tape to make it firmly stick on the coating surface. The peeling test experiments were then carried out by quickly peeling off the tape from the coating surface and were followed by a WCA measurement of the coating surface after sticking/peeling 5, 10, 50, 100, and 200 times.

2.8. Anticorrosion Experiment. AZ31B Mg alloy (2.5 cm × 1.0 cm × 0.05 cm), polished with 400 grit sandpaper to remove the passivation layer on the surface, was ultrasonically cleaned in acetone and ethanol for 30 min and then dried naturally in the air. The electrode of AZ31B Mg (Mg) was wrapped with tape except for the targeted exposed test area (1 cm^2) around the bottom, which was dipped in the electrolyte, as well as the top connection point. The designed coating was prepared by the spraying the dispersed solution of SiO_2@PSDP onto the Mg alloy and drying it in an oven at 60 °C for 6 h. A three-electrode electrochemical workstation system was adopted: the counter electrode is a platinum sheet, the reference electrode is silver/silver chloride (Ag/AgCl), and the working electrode is bare Mg alloy or coated Mg alloy (Mg/SiO_2@Poly(S-Myrcene-PFO), Mg/SiO_2@Poly(S-DCPD-PFO) and Mg/SiO_2@Poly(S-DIB-Octene)), and the electrolyte is composed of 3.5% NaCl aqueous solution. The Tafel curve at a rate of 10 mV/s of the exposed coating surface was then measured within a −2 to +1 V range to clarify the anticorrosion effect.

2.9. Antibacterial Experiment. The antibacterial activity of SiO_2@PSDP nanoparticles was evaluated by the plate count method. Gram-positive *S. aureus* and Gram-negative *E. coli* were selected as representative bacterial strains. Single colonies of *E. coli* and *S. aureus* strain were selected from the Luria−Bertani (LB) agar plate and inoculated in an LB fluid nutrient medium (50 mL). Bacteria suspensions were grown under shaking (200 rpm) at 37 °C for 15 h. The suspensions were diluted by phosphate buffered saline (PBS) solution to acquire 106 CFU/mL bacteria samples. To evaluate the antibacterial properties of SiO_2@PSDP nanoparticles (10 mg, 200 μg/mL), they were cocultivated with bacteria, and the blank group, where only the bacteria solution was added without the sample, and the samples were run with a constant temperature shaking (200 rpm) at 37 °C for 6 h. After the culture is completed, PBS solution was used to dilute the culture solution continuously by 10 times (three dilution multiples of 10^5, 10^6, and 10^7), and then the resultant diluted solution (120 μL) was taken and spread evenly on the LB solid medium. The resultant plate was then placed in a constant temperature incubator at 37 °C for 18 h, observing and taking pictures to record the number of colonies. Each group was set up with 2 parallel repetitions. In addition, all samples and utensils in the experiment were sterilized in advance in a high-temperature and high-pressure steam sterilizer at 121 °C for 30 min.

3. RESULTS AND DISCUSSION

Synthesis and Characterization of SiO_2@PSDP. As micro-/nanoroughness is critical to the superhydrophobic property, SiO_2 nanoparticles (SiO_2) were used along with S_8, zinc diethyldithiocarbamate ($Zn(DTC)_2$), 1,3-diisopropenyl-

https://doi.org/10.1021/acsapm.2c00490
ACS Appl. Polym. Mater. XXXX, XXX, XXX−XXX

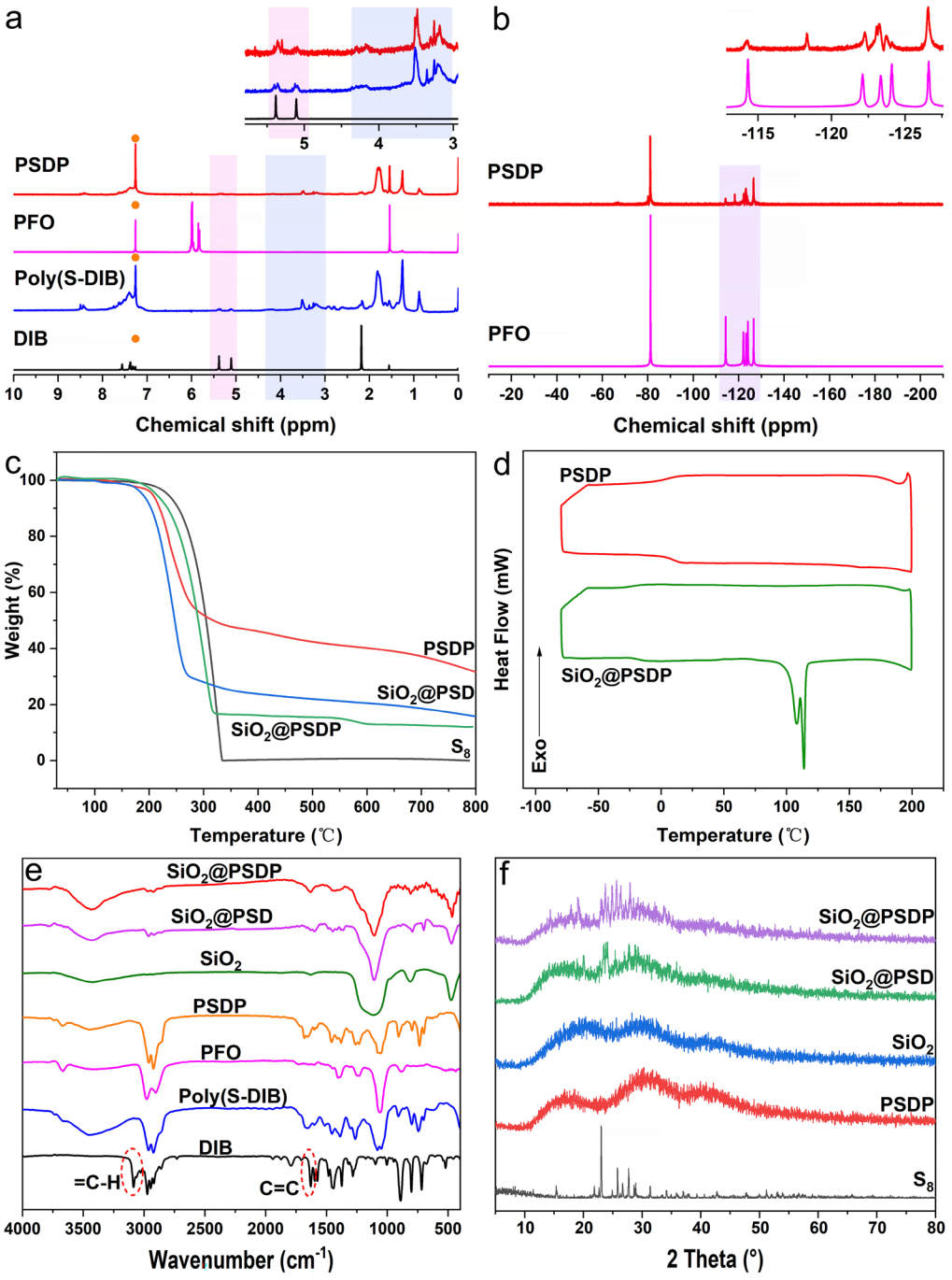

Figure 1. (a) ^{1}H NMR of the DIB, Poly(S-DIB), PFO, and PSDP. The illustration is an partial enlarged view of DIB, Poly(S-DIB) and PSDP, and the orange solid circle represents $CDCl_3$. (b) ^{19}F NMR of the PFO and PSDP. The illustration is an partial enlarged view of PFO and PSDP. (c) TGA thermograms of S_8, PSDP, SiO_2@PSD, and SiO_2@PSDP. (d) DSC thermograms of PSDP and SiO_2@PSDP. (e) FTIR spectra of DIB, Poly(S-DIB), PFO, PSDP, SiO_2, SiO_2@PSD, and SiO_2@PSDP. (f) PXRD spectra of S_8, PSDP, SiO_2, SiO_2@PSD, and SiO_2@PSDP.

benzene (DIB) and 1*H*,1*H*,2*H*-perfluoro-1-octene (PFO) in the order of sequence to form the coated SiO_2 copolymers SiO_2@Poly(S-DIB-PFO) (SiO_2@PSDP). Thus, SiO_2-embedded elemental sulfur was obtained by reacting sonicated SiO_2 (in DMF at 25 °C for 15 min) with S_8 under an inert atmosphere, presumably mainly by physical interaction via the van der Waals force between sulfur and the silica surface, so that sulfur is coated on SiO_2. Then, by the control of the reactant ratio, poly(S-DIB) was retained with SiO_2 nanoparticles via inverse vulcanization of the resultant SiO_2-embedded elemental sulfur with DIB in the present of $Zn(DTC)_2$ (1.5 wt %) based on a free radical polymerization mechanism.[2−10] Meanwhile, the external DIB segments hold a lower surface energy than the SiO_2 counterpart,[43] facilitating the coating with low surface energy monomer of PFO by the adoption of a tandem method under inert gas protection which prevents the free radicals from being adventitiously sacrificed by the oxygen in the air[44] and consequently generating SiO_2@Poly(S-DIB) (SiO_2@PSD) in a simple and easy way.[3] The obtained SiO_2@PSDP together with similar PSDP were characterized by NMR, FTIR, DSC, TGA, and PXRD spectrum analysis (Figure 1). In the ^{1}H NMR spectra, the

https://doi.org/10.1021/acsapm.2c00490
ACS Appl. Polym. Mater. XXXX, XXX, XXX−XXX

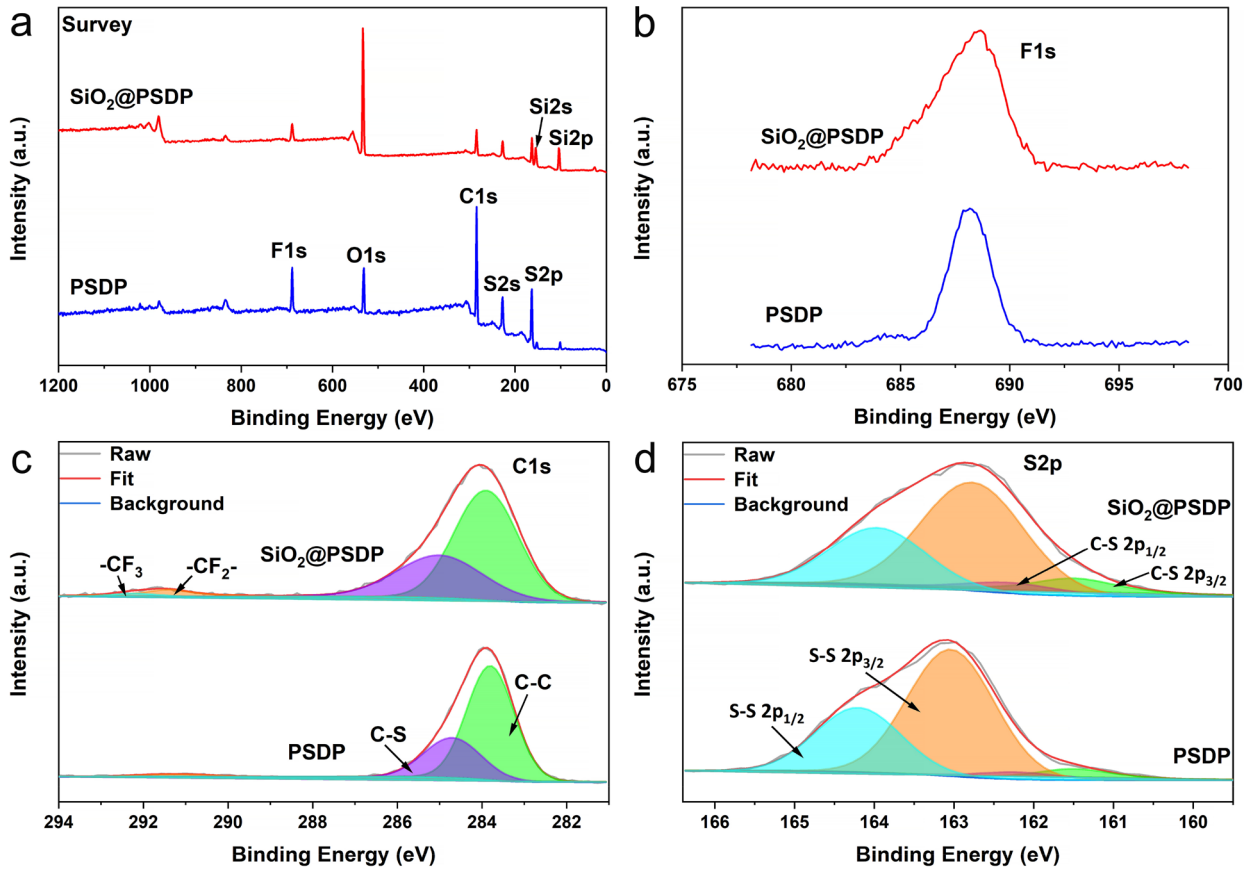

Figure 2. (a) XPS survey spectra of PSDP and SiO_2@PSDP. (b) F 1s spectra of PSDP and SiO_2@PSDP. (c) C 1s spectra of PSDP and SiO_2@PSDP. (d) S 2p spectra of PSDP and SiO_2@PSDP.

peaks of Poly(S-DIB) at 5.38 and 5.11 ppm are attributed to =C−H and $=CH_2$ of DIB, suggesting the existence of unreacted olefin double bonds after the inverse vulcanization of S_8 with DIB for 5 h; however, the peaks at 5.98 ppm (=C−H) and 5.82 ($=CH_2$) corresponding to PFO molecules completely disappeared, while the broad signals at 1−3 and 3−4.5 ppm belong to the alkane proton of CH_2 and S−C−H proton peaks in Poly(S-DIB) and PSDP,[13] evidencing the C−S covalent bond formation in the polymers together with the presence of peaks at around 56 ppm in ^{13}C NMR of both Poly(S-DIB) and PSDP for the newly formed C−S bond (Figure S7).[5,13] As shown in Figure 1b, compared to PFO, the broader peaks in ^{19}F NMR of PSDP indicated that polymerized PFO was present, presumably due to the chemical shifts from multiple fluorine atoms after polymerization. PSDP was reduced with $NaBH_4$ to further confirm its structure. There are no obvious peaks at the chemical shift of 3−4.5 ppm in ^1H NMR spectrum after reduction (Figures S1 and S2), indicating the absence of the previous S−C−H positions in the reduced PSDP. The M_n of the soluble fraction of the pristine PSDP was as high as 263000 g/mol, and it was decreased to 164000 g/mol after reduction. The possible reason for the decrease of the M_n for the reduced PSDP could be the S−S bond in the compound is reductively cleaved by the reducing reagent to obtain a polymer of DIB and PFO. These results revealed the success of well-designed PSDP copolymers tailored with PFO. There are no NMR spectra presented for SiO_2@PSDP due to the insufficient solubility. The identical ^1H NMR spectra of the poly(PFO) and poly(S-PFO) indicated no reaction occurred between S_8 and PFO (Figures S4−S6).

The thermogravimetric analysis (TGA) and differential scanning calorimetry (DSC) further confirmed the generation of designed polymers of PSDP and SiO_2@PSDP (Figures 1c,d). The 5% thermal decomposition temperature ($T_{deg,5\%}$) of obtained PSDP and SiO_2@PSDP is up to about 200 °C. Subsequently, the PSDP and SiO_2@PSDP undergo a process of weight loss of 45.4% and 79.6% before 330 °C due to the possible decomposition of sulfur bonds.[45] Compared to the continuous weight loss of PSDP after around 300 °C, negligible weight loss was observed for SiO_2@PSDP after a similar range of temperatures (330 °C), indicating that the cross-linked structure has a fairly stabilizing effect for nanoparticles. The slight weight loss at 550 °C possibly corresponded to the loss of the polymerized PFO as no such performance was observed for the similar composite of SiO_2@Poly(S-DIB) (Figure 1c). As shown in Figure 1d, compared with the glass transition temperature (T_g) of PSDP at 4.2 °C, a T_g of −11.9 °C was obtained for SiO_2@PSDP. The endothermic peaks of SiO_2@PSDP composite at 108.1 and 113.9 °C are likely attributed to the melting transitions (T_m) of the orthorhombic and monoclinic phases of the remaining sulfur ingredient.[3,45−47] It is probably due to the random extent polysulfide chains of the copolymer, indicating that a portion of the sulfur coated on SiO_2 was unable to fully participate in the inverse vulcanization.

The formation of PSDP, SiO_2@PSD, and SiO_2@PSDP was demonstrated by Fourier-transform infrared spectroscopy (FTIR) as well (Figure 1e). Compared to pristine DIB, the peaks at 3087 and 1630 cm^{-1} bands of the Poly(S-DIB) attributed to =C−H and $=CH_2$ were diminished or entirely

https://doi.org/10.1021/acsapm.2c00490
ACS Appl. Polym. Mater. XXXX, XXX, XXX−XXX

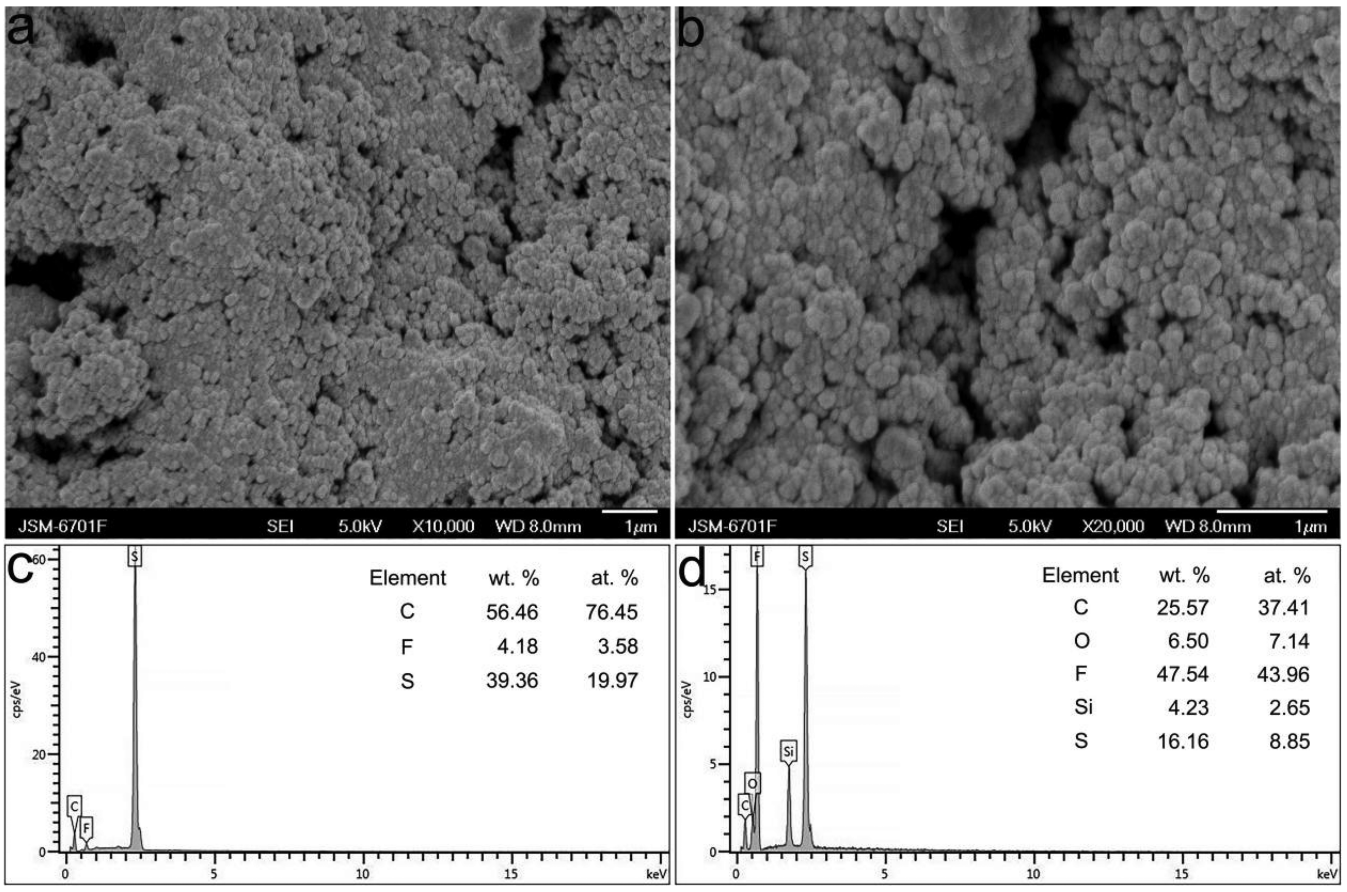

Figure 3. SEM images of SiO_2@PSDP (a, b); EDS image of PSDP (c); EDS image of SiO_2@PSDP (d).

gone, and a new peak at 622 cm^{-1} was noticed, belonging to the newly formed C−S bonds. The peaks at 1376 and 1250 cm^{-1} in the PSDP, SiO_2@PSD, and SiO_2@PSDP were assigned to C−C and C−F bonds stretching vibrations. The strong absorption band of SiO_2@PSD and SiO_2@PSDP at 3600−3200 cm^{-1} is ascribed to the stretching vibration peak of Si−OH, similar to that of SiO_2. Aligned to PSDP, two new strong bands appeared at 1112 and 809 cm^{-1} corresponded to Si−O−Si stretching of SiO_2@PSD and SiO_2@PSDP,[48−50] and the absorption peak at 475 cm^{-1} originated from the bending vibration peak of Si−O. All these data support that SiO_2@PSD and SiO_2@PSDP were synthesized successfully.

The X-ray powder diffraction (PXRD, Figure 1f) shows that there are no obvious characteristic diffraction patterns in PSDP, indicating that the crystalline octatomic S_8 is transformed into an amorphous polysulfide chain interior to the polymer skeleton. However, there are obvious S_8 diffraction peaks in SiO_2@PSD and SiO_2@PSDP, showing that the existence of unreacted S_8 coated on the surface of SiO_2 nanoparticles persisted but presented no barrier to the formation of the designed polymer-coated SiO_2 nanoparticles.

The introduction of TEMPO or BHT, a free radical scavenger, into the reaction system revealed that the PFO is initiated by the active free radicals existing in Poly(S-DIB) coated on the SiO_2 nanoparticles (Figure S16).

The chemical composition and bonding state of the SiO_2@PSDP coating were further verified by X-ray photoelectron spectroscopy (XPS) and illuminated the mechanism of wettability change. As shown in Figure 2a, the XPS survey spectrum from PSDP is mainly composed of C, O, F, and S elements,[25,51] while the spectrum for SiO_2@PSDP shows obvious O 1s (40.08%, at. %) and Si 2p (19.09, at. %) signal peaks at 533.1 and 103.9 eV,[52,53] the atomic ratio of element O to Si is about 2:1. For the high-resolution spectrum of the C 1s electrons (Figure 2c), the peaks at 283.9, 285.0, 291.4, and 292.2 eV are identified and corresponded to C−C, C−S, $-CF_2-$, and $-CF_3$ groups of SiO_2@PSDP.[25,51,54,55] Compared to PSDP, a slight change of the binding energy of the aforementioned elements was observed for the introduction of SiO_2 into SiO_2@PSDP. Analogously, the high-resolution S 2p spectrum (Figure 2d) shows that SiO_2@PSDP can be deconvoluted into four peaks at 161.5, 162.3, 162.8, and 164.0 eV whereas the binding energies of the S $2p_{3/2}$ (161.5 eV) and S $2p_{1/2}$ (162.3 eV) are assigned to the C−S bond, and the binding energies of S $2p_{3/2}$ (162.8 eV) and S $2p_{1/2}$ (164.0 eV) belong to the S−S linkage.[45,56] The existence of C−S and S−S bonds signified the formation of linear sulfur bridges for the S_8 ring after inverse vulcanization. The results of XPS further clarified that abundant low surface energy PFO groups were successfully grafted on the surface of SiO_2@Poly(S-DIB), which is a key factor for the building of superhydrophobic coatings. However, the physisorbing of polymers onto the SiO_2 indicates favorable intermolecular interactions between them.

To test the scope of the current protocol and examine the property-structure correlations, a series of similar polymers were synthesized by the same procedure, such as Poly(S-Myrcene) vs Poly(S-Myrcene-PFO), Poly(S-DCPD) vs Poly-(S-DCPD-PFO), and Poly(S-DIB-Octene) as well as all of them coated onto SiO_2 counterparts, and all the polymers and composites were characterized by ^1H NMR, FTIR, TGA, and

https://doi.org/10.1021/acsapm.2c00490
ACS Appl. Polym. Mater. XXXX, XXX, XXX−XXX

Table 1. Wettability (WCA) as a Function of the Amount of SiO_2, S_8, DIB, and PFO with Different Ratios

entry	SiO_2/mg	S:DIB:PFO/mol	S/mmol	DIB/mmol	PFO/mmol	WCA/deg
1	–	1:1:0	1	1	–	102.5 ± 7.2
2	50	1:1:0	1	1	–	125.3 ± 1.7
3	50	1.25:1.25:0	1.25	1.25	–	132.5 ± 2.4
4	50	1.5:1.5:0	1.5	1.5	–	134.6 ± 2.8
5	50	2:2:0	2	2	–	139.4 ± 0.8
6	50	1:1:1	1	1	1	136.5 ± 1.0
7	50	1.25:1.25:1.25	1.25	1.25	1.25	135.2 ± 1.6
8	50	1.5:1.5:1.5	1.5	1.5	1.5	136.0 ± 1.7
9	50	2:2:2	2	2	2	140.6 ± 2.1
10	30	1:1:1	1	1	1	106.1 ± 1.6
11	50	1:1:1	1	1	1	136.5 ± 1.0
12	80	1:1:1	1	1	1	137.1 ± 0.5
13	100	1:1:1	1	1	1	139.8 ± 0.5
14	120	1:1:1	1	1	1	142.6 ± 0.5
15	150	1:1:1	1	1	1	142.1 ± 1.7
16	120	0.8:1:1	0.8	1	1	123.6 ± 2.1
17	120	1.1:1:1	1.1	1	1	141.6 ± 3.7
18	120	1.2:1:1	1.2	1	1	144.2 ± 2.4
19	120	1.3:1:1	1.3	1	1	149.5 ± 1.8
20	120	1.4:1:1	1.4	1	1	154.7 ± 1.8
21	120	1.5:1:1	1.5	1	1	140.4 ± 1.3
22	120	1.6:1:1	1.6	1	1	145.3 ± 1.3
23	120	1.4:0.8:1	1.4	0.8	1	112.2 ± 1.5
24	120	1.4:0.9:1	1.4	0.9	1	124.8 ± 1.2
25	120	1.4:1.1:1	1.4	1.1	1	147.2 ± 1.6
26	120	1.4:1.2:1	1.4	1.2	1	146.0 ± 0.7
27	120	1.4:1.3:1	1.4	1.3	1	148.1 ± 1.5
28	120	1.4:1:0.8	1.4	1	0.8	148.5 ± 1.6
29	120	1.4:1:0.9	1.4	1	0.9	152.3 ± 0.7
30	120	1.4:1:1.1	1.4	1	1.1	151.1 ± 2.7
31	120	1.4:1:1.2	1.4	1	1.2	150.7 ± 2.1
32	120	1.4:1:1.3	1.4	1	1.3	147.3 ± 0.9
33	120	1.4:1:1.4	1.4	1	1.4	146.8 ± 0.1

PXRD (Figures S8–S15). ^{1}H NMR, FTIR, and PXRD showed the possible synthesis of the corresponding analogues, and the $T_{deg,5\%}$ of similar materials synthesized with other cross-linkers such as myrcene, DCPD, and SiO_2@Poly(S-DIB-Octene) reached 180 °C.

Morphological and Elemental Composition Analyses. The surface morphology and element composition of PSDP and SiO_2@PSDP were evaluated by Scanning Electron Microscopy (SEM) and Energy-Dispersive X-ray Spectroscopy (EDS). The surface of the SiO_2@PSDP substrate becomes rough, and significant microspheres were scattered (Figure 3a,b). These shapes and structures are conducive to the fine superhydrophobic features of the materials. The presence of C, F, and S elements in PSDP was found in the corresponding EDS (Figure 3c) analysis. The EDS spectrum of SiO_2@PSDP (Figure 3d) demonstrated that the characteristic elements of the coating surface include C, O, F, Si, and S atoms, with a dramatic increase of the F element content. It is supported that the coating surface contains a large quantity of PFO segments, further proving the successful formation of designed PSDP encapsulated SiO_2 nanoparticles.

Contact Angle Measurement. The wettability of the material surface, a property of which SiO_2@PSDP was designed with in mind, is a distinguishing feature to its actual application, namely, the superhydrophobic surface furnishing the aforementioned advantages such as self-cleaning and corrosion resistance. Spraying technology is conducive to the preparation of large-scale superhydrophobic surfaces, and the wettability of SiO_2@PSDP coated glass substrates using such technology was assessed by the measurement of static contact angle. Compared to the Water Contact Angle (WCA) of the original Poly(S-DIB) at 102.5 ± 7.2°. Significant increases were secured with the embedded SiO_2 in the polymers (entries 1 vs 2–8, Table 1). Interestingly, a WCA of 136.5 ± 1.0° was observed for the addition of PFO into the polymer (entry 5, Table 1), with a lesser amount of polymer addition as the optimum. The decline in micro-/nanoroughness caused by the increased amount of PFO in the polymer could lower the superhydrophobicity dominantly. Subsequently, the impact factors on superhydrophobicity, such as cross-linking, monomers, and SiO_2, were systematically investigated (Table 1). As expected, the amounts of SiO_2, S_8, DIB, and PFO all have pronounced effects on the superhydrophobicity of the resultant polymers and so do their ratios. Therefore, a maximum corresponding WCA of up to 142.6 ± 0.5° was achieved with 120 mg of SiO_2, and 154.7 ± 1.8° for 1.4 mmol of the S_8 used. The optimal reagent quantity of SiO_2 at this reaction scale is 120 mg, which combined with a molar ratio of 1.4:1:1 S:DIB:PFO, gives the best material reported here, in terms of contact angle. The wetting properties of different substances coated on SiO_2 nanoparticles were studied (Table S2), and the superhydrophobic SiO_2@PSDP coating was consequently

https://doi.org/10.1021/acsapm.2c00490
ACS Appl. Polym. Mater. XXXX, XXX, XXX−XXX

prepared by a spraying method as reported in literature,[57] with PFO directly affecting the wetting properties of SiO_2-based composites.

The scope of the cross-linkers and the property-structure correlations for the superhydrophobicity of SiO_2 embedded polymers were conducted by the replacement of DIB with other olefins (Tables S3 and S4; Figures S3 and S4). Thus, with the optimal ratio of SiO_2@PSDP, the WCA of SiO_2@Poly(S-Myrcene-PFO) reaches 136.5 ± 1.0° when the myrcene is used (Table S3), and a further increase up to 148.9 ± 0.5° could be obtained with a high portion of poly(S-Myrcene). Interestingly, with a rigid and cyclic cross-linker, DCPD, the WCA can reach up to 150.5 ± 1.7° under optimized conditions (Table S4). Of particular note is that the low surface energy PFO replaced with olefin 1-octene, the same carbon chain length analogue, afforded a similar SiO_2@Poly(S-DIB-Octene) composite with the WCA of 130.5 ± 2.2°, indicating the important role of PFO in the wetting performance (Table S5). The primary results suggested that cross-linkers with aromatic structure afforded higher WCA than the aliphatic counterpart, as was also observed for the superhydrophobicity.

The self-cleaning characteristic is another key functionality of the superhydrophobic surface, and it has super advantages in practical applications. The self-cleaning of the SiO_2@PSDP coating was evaluated by spraying the SiO_2@PSDP on the glass slide placed slantwise. After a little sand was sprinkled onto the SiO_2@PSDP coating surface, water droplets were rinsed onto it to examine the self-cleaning performance, recording by a digital camera for this self-cleaning process (Video S1).[58] It was found that the surface of the superhydrophobic coating becomes clean again with the water droplets able to roll and return to the original standard without any moisture remaining, indicating an excellent self-cleaning and superhydrophobic performance of the surface of SiO_2@PSDP. At the same time, the mechanical properties of the material were qualitatively tested by peeling experiments, and the WCA decreased from 154.7 ± 1.8° to 138.2 ± 0.2° when the number of peeling times reached 200, but the coating still possessed hydrophobicity (Table S6).

Corrosion Resistance of the SiO_2@PSDP Coating. The anticorrosion performance of SiO_2@PSDP coatings was subsequently evaluated by the Tafel polarization curve method (Figure 4). To simulate the corrosion of the coating on magnesium alloy (Mg, 2.5 cm × 1.0 cm × 0.05 cm) in seawater (3.5 wt % NaCl), the corrosion current density (I_{corr}) and corrosion potential (E_{corr}) were measured (Table S7). Compared to the bare Mg alloy, the I_{corr} of the coated Mg alloy is significantly decreased 2 orders of magnitude; that is from 1.704×10^{-4} to 1.809×10^{-6} A·cm^{-2}. The E_{corr} of the coated Mg alloy samples shifted approximately 111 mV to the positive direction. These results demonstrated that the composite SiO_2@PSDP coating dramatically increased the corrosion resistance of Mg alloy sheets. The corresponding coating protection rate (η) of the SiO_2@PSDP coating is as high as 98.9% as calculated by formula 1.[53]

$$\eta = \frac{I_{corr0} - I_{corr}}{I_{corr0}} \times 100\% \quad (1)$$

Here I_{corr0} and I_{corr} are the current density of bare Mg alloy and SiO_2@PSDP coating, respectively. The similar materials synthesized with other cross-linkers such as myrcene and DCPD furnish excellent protection rate at the same level (97.2% and 97.3% respectively), and SiO_2@Poly(S-DIB-Octene) coating also reached 95.2%, evidencing the outstanding corrosion resistance property of these SiO_2 embedded materials.

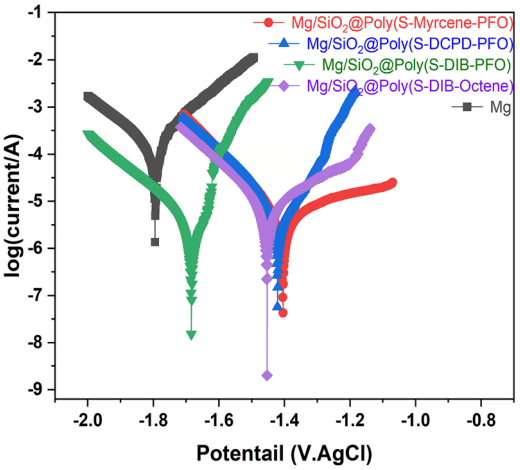

Figure 4. Polarization curves of the Mg, SiO_2@Poly(S-Myrcene-PFO), SiO_2@Poly(S-DCPD-PFO), and SiO_2@Poly(S-DIB-Octene) samples in 3.5 wt % NaCl solution.

Antibacterial Activity of SiO_2@PSDP. The antibacterial properties of SiO_2@PSDP were measured by the plate count method (Figure 5, Table S8). Gram-positive bacteria *S. aureus* and Gram-negative bacteria *E. coli* were conducted as representative strains. As shown in Table S9, the inhibitory rates of 81% against *S. aureus* and 75% against *E. coli* were achieved with the concentration of dispersed SiO_2@PSDP at 200 μg/mL, stipulating a good antibacterial effect against both *S. aureus* and *E. coli*.[34,35,59]

4. CONCLUSIONS

In summary, a simple approach to develop SiO_2 embedded S-rich polymers by means of the inverse vulcanization process tailored with functional groups was verified, revealing superhydrophobicity, anticorrosion, and antibacterial properties of the resultant composites. Starting with coating onto SiO_2 nanoparticles, the S_8 was introduced into polymer chains through the inverse vulcanization to generate SiO_2@Poly(S-DIB) and reduce the high surface energy of SiO_2. This facilitated the low surface energy PFO coating on SiO_2@Poly(S-DIB) to generate SiO_2@PSDP. The SiO_2@PSDP coating has good to excellent properties of superhydrophobicity (WCA of 154.7 ± 1.8°), self-cleaning, antibacterial, and anticorrosive properties. The SiO_2@PSDP suspension was sprayed on the glass slide and magnesium alloy surface to form a superhydrophobic coating. The microstructures and thermal properties of the SiO_2@PSDP coating were characterized. Meantime, a protection efficiency up to 98.9% for magnesium alloy in 3.5% NaCl was achieved. The antibacterial activity experiment showed that the antibacterial rate against *S. aureus* and *E. coli* reached 81.4% and 74.6%, respectively. This simple strategy offers a valuable method for constructing superhydrophobic, antibacterial, and anticorrosive coatings materials, further expanding application areas for sulfur-rich polymers resulting from inverse vulcanization as well as providing low-cost alternatives to superhydrophobic coating materials.

https://doi.org/10.1021/acsapm.2c00490
ACS Appl. Polym. Mater. XXXX, XXX, XXX−XXX

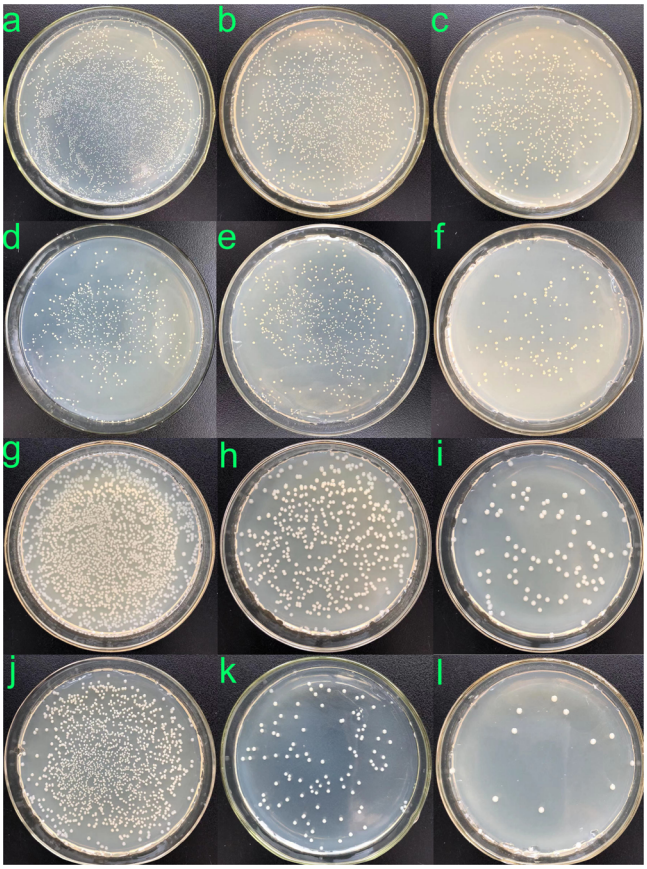

Figure 5. Representative colonies of *S. aureus* formed on LB agar plates in the presence of (a–c) PBS solution and (d–f) SiO_2@PSDP. Parts a-c and d–f were serial 10-fold dilutions. Representative colonies of *E. coli* formed on LB agar plates in the presence of (g–i) PBS solution and (j–l) SiO_2@PSDP. Parts g–i and j–l were serial 10-fold dilutions.

■ ASSOCIATED CONTENT

Supporting Information

The Supporting Information is available free of charge at https://pubs.acs.org/doi/10.1021/acsapm.2c00490.

Self-cleaning performance (Video S1) (MP4)

■ AUTHOR INFORMATION

Corresponding Authors

Jian Li − *College of Chemistry and Chemical Engineering, Gansu International Scientific and Technological Cooperation Base of Water-Retention Chemical Functional Material, Northwest Normal University, Lanzhou 730070, P. R. China;* orcid.org/0000-0001-5104-1564; Email: jianli83@126.com

Xiaofeng Wu − *College of Chemistry and Chemical Engineering, Gansu International Scientific and Technological Cooperation Base of Water-Retention Chemical Functional Material, Northwest Normal University, Lanzhou 730070, P. R. China; Department of Chemistry, University of Liverpool, Liverpool L69 7ZD, U.K.;* orcid.org/0000-0001-5549-8836; Email: xfwu@liverpool.ac.uk

Tom Hasell − *College of Chemistry and Chemical Engineering, Gansu International Scientific and Technological Cooperation Base of Water-Retention Chemical Functional Material, Northwest Normal University, Lanzhou 730070, P. R. China; Department of Chemistry, University of Liverpool, Liverpool L69 7ZD, U.K.;* orcid.org/0000-0003-4736-0604; Email: t0m@liverpool.ac.uk

Zheng-Jun Quan − *College of Chemistry and Chemical Engineering, Gansu International Scientific and Technological Cooperation Base of Water-Retention Chemical Functional Material, Northwest Normal University, Lanzhou 730070, P. R. China;* orcid.org/0000-0002-4393-3594; Email: quanzhengjun@hotmail.com

Authors

Congcong Miao − *College of Chemistry and Chemical Engineering, Gansu International Scientific and Technological Cooperation Base of Water-Retention Chemical Functional Material, Northwest Normal University, Lanzhou 730070, P. R. China*

Xingwei Xun − *College of Chemistry and Chemical Engineering, Gansu International Scientific and Technological Cooperation Base of Water-Retention Chemical Functional Material, Northwest Normal University, Lanzhou 730070, P. R. China*

Liam J. Dodd − *Department of Chemistry, University of Liverpool, Liverpool L69 7ZD, U.K.*

Shiquan Niu − *College of Life Sciences, Northwest Normal University, Lanzhou 730070, P. R. China*

Haoran Wang − *Department of Chemistry, University of Liverpool, Liverpool L69 7ZD, U.K.*

Peiyao Yan − *Department of Chemistry, University of Liverpool, Liverpool L69 7ZD, U.K.*

Xi-Cun Wang − *College of Chemistry and Chemical Engineering, Gansu International Scientific and Technological Cooperation Base of Water-Retention Chemical Functional Material, Northwest Normal University, Lanzhou 730070, P. R. China*

Complete contact information is available at: https://pubs.acs.org/10.1021/acsapm.2c00490

Author Contributions

C.M. designed, synthesized, and characterized the materials as well as performed the applications. X.X. performed mechanical properties measurement. S.N. and J.L., provided methods and instruments for the antibacterial and WCA functionality test. L.J.D., H.W., and P.Y. performed the DSC, TGA, PXRD, and FTIR measurements and assisted with interpretation. X.-C.W. assisted with the anticorrosion performance testing. X.W., T.H., and Z.-J.Q. directed the project. Data analysis and manuscript preparation were written through contributions of all authors. All authors have given approval to the final version of the manuscript.

Notes

The authors declare no competing financial interest.

■ ACKNOWLEDGMENTS

We are thankful for the financial support from the National Nature Science Foundation of China (NSFC, 22067018, 22101232), the Natural Science Foundation of Gansu Province (20YF3GA023), and the Programme of Introducing Talents of Discipline to Universities (No. B16017). H.W and P. Y. thank the China Scholarship Council for studentship support. T.H. was supported by a Royal Society University Research Fellowship. The authors are also very grateful to the Materials

https://doi.org/10.1021/acsapm.2c00490
ACS Appl. Polym. Mater. XXXX, XXX, XXX−XXX

Innovation Factory (MIF) team members for their support in operating instruments.

REFERENCES

(1) Boyd, D. A. Sulfur and its role in modern materials science. *Angew. Chem., Int. Ed.* **2016**, *55*, 15486−15502.
(2) Griebel, J. J.; Glass, R. S.; Char, K.; Pyun, J. Polymerizations with elemental sulfur: a novel route to high sulfur content polymers for sustainability, energy and defense. *Prog. Polym. Sci.* **2016**, *58*, 90−125.
(3) Chung, W. J.; Griebel, J. J.; Kim, E. T.; Yoon, H.; Simmonds, A. G.; Ji, H. J.; Dirlam, P. T.; Glass, R. S.; Wie, J. J.; Nguyen, N. A.; Guralnick, B. W.; Park, J.; Somogyi, A.; Theato, P.; Mackay, M. E.; Sung, Y. E.; Char, K.; Pyun, J. The use of elemental sulfur as an alternative feedstock for polymeric materials. *Nat. Chem.* **2013**, *5*, 518−524.
(4) Worthington, M. J. H.; Kucera, R. L.; Chalker, J. M. Green chemistry and polymers made from sulfur. *Green Chem.* **2017**, *19*, 2748−2761.
(5) Zhang, Y. Y.; Glass, R. S.; Char, K.; Pyun, J. Recent advances in the polymerization of elemental sulphur, inverse vulcanization and methods to obtain functional Chalcogenide Hybrid Inorganic/Organic Polymers (CHIPs). *Polym. Chem.* **2019**, *10*, 4078−4105.
(6) Zhu, Y. Q.; Romain, C.; Williams, C. K. Sustainable polymers from renewable resources. *Nature* **2016**, *540*, 354−362.
(7) Chalker, J. M.; Worthington, M. J. H.; Lundquist, N. A.; Esdaile, L. J. Synthesis and applications of polymers made by inverse vulcanization. *Top. Curr. Chem.* **2019**, *377*, 16.
(8) Ghumman, A. S. M.; Nasef, M. M.; Shamsuddin, M. R.; Abbasi, A. Evaluation of properties of sulfur-based polymers obtained by inverse vulcanization: Techniques and challenges. *Polym. Polym. Compos.* **2021**, *29* (8), 1333−1352.
(9) Wu, X. F.; Smith, J. A.; Petcher, S.; Zhang, B. W.; Parker, D. J.; Griffin, G. M.; Hasell, T. Catalytic inverse vulcanization. *Nat. Commun.* **2019**, *10*, 647.
(10) Dodd, L. J.; Omar, O.; Wu, X. F.; Hasell, T. Investigating the role and scope of catalysts in inverse vulcanization. *ACS Catal.* **2021**, *11*, 4441−4455.
(11) Crockett, M. P.; Evans, A. M.; Worthington, M. J. H.; Albuquerque, I. S.; Slattery, A. D.; Gibson, C. T.; Campbell, J. A.; Lewis, D. A.; Bernardes, G. J. L.; Chalker, J. M. Sulfur-limonene polysulfide: a material synthesized entirely from industrial by-products and its use in removing toxic metals from water and soil. *Angew. Chem., Int. Ed.* **2016**, *55*, 1714−1718.
(12) Worthington, M. J. H.; Kucera, R. L.; Albuquerque, I. S.; Gibson, C. T.; Sibley, A.; Slattery, A. D.; Campbell, J. A.; Alboaiji, S. F. K.; Muller, K. A.; Young, J.; Adamson, N.; Gascooke, J. R.; Jampaiah, D.; Sabri, Y. M.; Bhargava, S. K.; Ippolito, S. J.; Lewis, D. A.; Quinton, J. S.; Ellis, A. V.; Johs, A.; Bernardes, G. J. L.; Chalker, J. M. Laying waste to mercury: inexpensive sorbents made from sulfur and recycled cooking oils. *Chem. Eur. J.* **2017**, *23*, 16219−16230.
(13) Parker, D. J.; Jones, H. A.; Petcher, S.; Cervini, L.; Griffin, J. M.; Akhtar, R.; Hasell, T. Low cost and renewable sulfur-polymers by inverse vulcanisation, and their potential for mercury Capture. *J. Mater. Chem. A* **2017**, *5*, 11682−11692.
(14) Worthington, M. J. H.; Shearer, C. J.; Esdaile, L. J.; Campbell, J. A.; Gibson, C. T.; Legg, S. K.; Yin, Y. T.; Lundquist, N. A.; Gascooke, J. R.; Albuquerque, I. S.; Shapter, J. G.; Andersson, G. G.; Lewis, D. A.; Bernardes, G. J. L.; Chalker, J. M. Sustainable polysulfides for oil spill remediation: repurposing industrial waste for environmental benefit. *Adv. Sust. Syst.* **2018**, *2*, 1800024.
(15) Abraham, A. M.; Kumar, S. V.; Alhassan, S. M. Porous sulphur copolymer for gas-phase mercury removal and thermal Insulation. *Chem. Eng. J.* **2018**, *332*, 1−7.
(16) Lundquist, N. A.; Worthington, M. J. H.; Adamson, N.; Gibson, C. T.; Johnston, M. R.; Ellis, A. V.; Chalker, J. M. Polysulfides made from re-purposed waste are sustainable materials for removing iron from water. *RSC Adv.* **2018**, *8*, 1232−1236.
(17) Tikoalu, A. D.; Lundquist, N. A.; Chalker, J. M. Mercury sorbents made by inverse vulcanization of sustainable triglycerides: the plant oil structure influences the rate of mercury removal from water. *Adv. Sust. Syst.* **2020**, *4*, 1900111.
(18) Zhang, Y. Y.; Griebel, J. J.; Dirlam, P. T.; Nguyen, N. A.; Glass, R. S.; Mackay, M. E.; Char, K.; Pyun, J. Inverse vulcanization of elemental sulfur and styrene for polymeric cathodes in Li-S Batteries. *J. Polym. Sci. A Polym. Chem.* **2017**, *55*, 107−116.
(19) Hoefling, A.; Lee, Y. J.; Theato, P. Sulfur-based polymer composites from vegetable oils and elemental sulfur: a sustainable active material for Li-S batteries. *Macromol. Chem. Phys.* **2017**, *218*, 1600303.
(20) Gomez, I.; Mecerreyes, D.; Blazquez, J. A.; Leonet, O.; Ben Youcef, H.; Li, C. M.; Gomez-Camer, J. L.; Bondarchuk, O.; Rodriguez-Martinez, L. Inverse vulcanization of sulfur with divinylbenzene: Stable and easy processable cathode material for lithium-sulfur batteries. *J. Power Sources* **2016**, *329*, 72−78.
(21) Gomez, I.; Leonet, O.; Alberto Blazquez, J.; Grande, H. J.; Mecerreyes, D. Poly(anthraquinonyl sulfides): high capacity redox polymers for energy storage. *ACS Macro. Lett.* **2018**, *7*, 419−424.
(22) Shukla, S.; Ghosh, A.; Sen, U. K.; Roy, P. K.; Mitra, S.; Lochab, B. Cardanol benzoxazine-sulfur copolymers for Li-S batteries: symbiosis of sustainability and performance. *ChemistrySelect* **2016**, *1*, 594−600.
(23) Gomez, I.; Leonet, O.; Blazquez, J. A.; Mecerreyes, D. Inverse vulcanization of sulfur using natural dienes as sustainable materials for lithium-sulfur batteries. *ChemSusChem* **2016**, *9*, 3419−3425.
(24) Zeng, S. B.; Li, L. G.; Yu, J. P.; Wang, N.; Chen, S. W. Highly crosslinked organosulfur copolymer nanosheets with abundant mesopores as cathode materials for efficient lithium-sulfur batteries. *Electrochim. Acta* **2018**, *263*, 53−59.
(25) Li, L. G.; Zeng, S. B.; Xie, L. H.; Zhao, D. K.; Wang, N.; Chen, S. W. Conducting polymers crosslinked with sulfur as cathode materials for high-rate, ultralong-life lithium-sulfur batteries. *ChemSusChem* **2017**, *10*, 3378−3386.
(26) Kang, H.; Kim, H.; Park, M. J. Sulfur-rich polymers with functional linkers for high-capacity and fast-charging lithium-sulfur batteries. *Adv. Energy Mater.* **2018**, *8*, 1802423.
(27) Valle, S. F.; Giroto, A. S.; Klaic, R.; Guimarães, G. G. F.; Ribeiro, C. Sulfur fertilizer based on inverse vulcanization process with soybean oil. *Polym. Degrad. Stab.* **2019**, *162*, 102−105.
(28) Mann, M.; Kruger, J. E.; Andari, F.; McErlean, J.; Gascooke, J. R.; Smith, J. A.; Worthington, M. J. H.; McKinley, C. C. C.; Campbell, J. A.; Lewis, D. A.; Hasell, T.; Perkins, M. V.; Chalker, J. M. Sulfur polymer composites as controlled-release fertilisers. *Org. Biomol. Chem.* **2019**, *17*, 1929−1936.
(29) Griebel, J. J.; Nguyen, N. A.; Astashkin, A. V.; Glass, R. S.; Mackay, M. E.; Char, K.; Pyun, J. Preparation of dynamic covalent polymers via inverse vulcanization of elemental sulfur. *ACS Macro. Lett.* **2014**, *3*, 1258−1261.
(30) Griebel, J. J.; Namnabat, S.; Kim, E. T.; Himmelhuber, R.; Moronta, D. H.; Chung, W. J.; Simmonds, A. G.; Kim, K. J.; van der Laan, J.; Nguyen, N. A.; Dereniak, E. L.; Mackay, M. E.; Char, K.; Glass, R. S.; Norwood, R. A.; Pyun, J. New infrared transmitting material via inverse vulcanization of elemental sulfur to prepare high refractive index polymers. *Adv. Mater.* **2014**, *26*, 3014−3018.
(31) Griebel, J. J.; Nguyen, N. A.; Namnabat, S.; Anderson, L. E.; Glass, R. S.; Norwood, R. A.; Mackay, M. E.; Char, K.; Pyun, J. Dynamic covalent polymers via inverse vulcanization of elemental sulfur for healable infrared optical materials. *ACS Macro. Lett.* **2015**, *4*, 862−866.
(32) Xin, Y. M.; Peng, H.; Xu, J.; Zhang, J. Y. Ultrauniform embedded liquid metal in sulfur polymers for recyclable, conductive, and self-healable materials. *Adv. Funct. Mater.* **2019**, *29*, 1808989.
(33) Lin, H. K.; Liu, Y. L. Reactive hybrid of polyhedral oligomeric silsesquioxane (POSS) and sulfur as a building block for self-Healing materials. *Macromol. Rapid Commun.* **2017**, *38*, 1700051.
(34) Deng, Z. L.; Hoefling, A.; Théato, P.; Lienkamp, K. Surface properties and antimicrobial activity of poly(sulfur-co-1,3-diisopropenylbenzene) copolymers. *macromol. Chem. Phys.* **2018**, *219*, 1700497.

https://doi.org/10.1021/acsapm.2c00490
ACS Appl. Polym. Mater. XXXX, XXX, XXX−XXX

(35) Smith, J. A.; Mulhall, R.; Goodman, S.; Fleming, G.; Allison, H.; Raval, R.; Hasell, T. Investigating the antibacterial properties of inverse vulcanized sulfur polymers. *ACS Omega* **2020**, *5*, 5229−5234.
(36) Chen, H. Y.; Fan, H. Z.; Su, N.; Hong, R. Y.; Lu, X. S. Highly hydrophobic polyaniline nanoparticles for anti-corrosion epoxy coatings. *Chem. Eng. J.* **2021**, *420*, 130540.
(37) Wen, S. F.; Wang, P.; Wang, L. Preparation and antifouling performance evaluation of fluorine-containing amphiphilic silica nanoparticles. *Colloids Surf. A Physicochem. Eng. Aspects* **2021**, *611*, 125823.
(38) Zheng, H. P.; Li, Z.; Liu, L.; Meng, F. D.; Cui, Y.; Wang, F. H. Superhydrophobic composite coatings in bacterial culture media: Durable antibacterial activity and enhanced corrosion resistance. *Compos. Commun.* **2021**, *27*, 100857.
(39) Xu, H. D.; Fan, S. H.; Lu, Y.; Feng, H. X.; Qiu, J. H. Proposal and verification of a novel superhydrophobic-conductive anti-corrosion polyaniline-silica coating. *Bull. Chem. Soc. Jpn.* **2020**, *93*, 1114−1120.
(40) Ma, J. Z.; Liu, C. Y.; Yan, K. CQDs-MoS_2 QDs loaded on dendritic fibrous nanosilica/hydrophobic waterborne polyurethane acrylate for antibacterial coatings. *Chem. Eng. J.* **2022**, *429*, 132170.
(41) Suryaprabha, T.; Sethuraman, M. G. Fabrication of copper-based superhydrophobic self-cleaning antibacterial coating over cotton fabric. *Cellulose* **2017**, *24*, 395−407.
(42) Wen, H.; Raza, S.; Wang, P.; Zhu, Z. Y.; Zhang, J. Y.; Huang, W.; Liang, L. Z.; Hu, H.; Deng, L. B.; Liu, C. K. Robust super hydrophobic cotton fabrics functionalized with Ag and PDMS for effective antibacterial activity and efficient oil-water separation. *J. Environ. Chem. Eng.* **2021**, *9*, 106083.
(43) Wang, S. T.; Liu, K. S.; Yao, X.; Jiang, L. Bioinspired surfaces with superwettability: new insight on theory, design, and applications. *Chem. Rev.* **2015**, *115*, 8230−8293.
(44) Choi, J.; Won, S.; Yoon, H. J.; Lee, J. H.; Jang, H. W.; Jeon, J.; Kim, A. Y.; Park, S. H.; Youk, J. H.; Lee, M.; Wie, J. J. Toxic gas-free synthesis of extremely negative triboelectric sulfur copolymer blends via phase separation of fluorine-rich polymers. *Nano Energy* **2022**, *92*, 106761.
(45) Arslan, M.; Kiskan, B.; Yagci, Y. Toxic gas-free synthesis of extremely negative triboelectric sulfur copolymer blends via phase separation of fluorine-rich polymers. *Macromolecules* **2016**, *49*, 767−773.
(46) Liu, X.; Lu, Y.; Zeng, Q. H.; Chen, P. P.; Li, Z. F.; Wen, X.; Wen, W.; Li, Z. X.; Zhang, L. Y. Sulfur-rich poly (ionic liquid) cathode materials combining chemical connecting and cation electrostatic trapping of polysulfides for ultralong-life lithium sulfur batteries. *ChemSusChem* **2020**, *13*, 715−723.
(47) Ma, J. P.; Fan, J. B.; Chen, S.; Yang, X. Y.; Hui, K. N.; Zhang, H. W.; Bielawski, C. W.; Geng, J. X. Covalent confinement of sulfur copolymers onto graphene sheets affords ultrastable lithium-sulfur batteries with fast cathode kinetics. *ACS Appl. Mater. Interfaces* **2019**, *11*, 13234−13243.
(48) Chen, Z. Y.; Droste, J.; Zhai, G. Q.; Zhu, J. H.; Yang, J.; Hansen, M. R.; Zhuang, X. D. Sulfur-anchored azulene as a cathode material for Li-S batteries. *Chem. Commun.* **2019**, *55*, 9047−9050.
(49) Lin, X. H.; Yin, M. L.; Liu, Y.; Li, L.; Ren, X. H.; Sun, Y. Y.; Huang, T. S. Biodegradable polyhydroxybutyrate/poly-ε-caprolactone fibrous membranes modified by silica composite hydrol for super hydrophobic and outstanding antibacterial application. *J. Ind. Eng. Chem.* **2018**, *63*, 303−311.
(50) Jeon, Y.; Nagappan, S.; Li, X. H.; Lee, J. H.; Shi, L. Y.; Yuan, S.; Lee, W. K.; Ha, C. S. Highly transparent, robust hydrophobic, and amphiphilic organic-inorganic hybrid coatings for antifogging and antibacterial applications. *ACS Appl. Mater. Interfaces* **2021**, *13*, 6615−6630.
(51) Peng, J. W.; Yuan, S. C.; Geng, H. L.; Zhang, X. G.; Zhang, M.; Xu, F.; Lin, D.; Gao, Y. Y.; Wang, H. Y. Robust and multifunctional superamphiphobic coating toward effective anti-adhesion. *Chem. Eng. J.* **2022**, *428*, 131162.
(52) Qian, F. Y.; Zheng, Y. X.; Pan, N. Y.; Li, L.; Li, R.; Ren, X. H. Synthesis of polysiloxane and its co-application with nano-SiO_2 for antibacterial and hydrophobic cotton fabrics. *Cellulose* **2021**, *28*, 3169−3181.
(53) Li, D. W.; Wang, H. Y.; Liu, Y.; Wei, D. S.; Zhao, Z. X. Large-scale fabrication of durable and robust super-hydrophobic spray coatings with excellent repairable and anti-corrosion performance. *Chem. Eng. J.* **2019**, *367*, 169−179.
(54) Liu, J. L.; Zhu, Y. R.; Chen, X. H.; Yi, W. J. Nitrogen, sulfur and phosphorus tri-doped holey graphene oxide as a novel electrode material for application in supercapacitor-ScienceDirect. *J. Alloys Compd.* **2020**, *815*, 152328.
(55) Charles-Blin, Y.; Flahaut, D.; Ledeuil, J. B.; Guérin, K.; Dubois, M.; Deschamps, M.; Perbost, A. M.; Monconduit, L.; Martinez, H.; Louvain, N. Atomic layer fluorination of the $Li_4Ti_5O_{12}$ surface: a multiprobing survey. *ACS Appl. Energy Mater.* **2019**, *2*, 6681−6692.
(56) Kim, H.; Lee, J.; Ahn, H.; Kim, O.; Park, M. J. Synthesis of three-dimensionally interconnected sulfur-rich polymers for cathode materials of high-rate lithium-sulfur batteries. *Nat. Commun.* **2015**, *6*, 7278.
(57) Xu, H. D.; Wang, Y. L.; Zhao, D.; Chen, N. L.; Tan, L.; Feng, H. X. Based on TRIZ methodology design and preparation of a robust skeletal superhydrophobic perfluoropolysiloxane and polyaniline/epoxy resin composite coating with outstanding anti-corrosion performance. *Bull. Chem. Soc. Jpn.* **2021**, *94*, 2390−2395.
(58) Cao, W. T.; Liu, Y. J.; Ma, M. G.; Zhu, J. F. Facile preparation of robust and superhydrophobic materials for self-cleaning and oil/water separation. *Colloids Surf. A Physicochem. Eng. Aspects* **2017**, *529*, 18−25.
(59) Dop, R. A.; Neill, D. R.; Hasell, T. Antibacterial activity of inverse vulcanized polymers. *biomacromolecules* **2021**, *22*, 5223−5233.

https://doi.org/10.1021/acsapm.2c00490
ACS Appl. Polym. Mater. XXXX, XXX, XXX−XXX